The 2021 Antarctic Total Eclipse: Ground Magnetometer and GNSS Wave Observations from the 40 Degree Magnetic Meridian

Shane Coyle[1], Michael D. Hartinger[2], C. Robert Clauer[3], J. B. H. Baker[1], Ingrid Cnossen[4], Mervyn P. Freeman[4], and James M. Weygand[5]

[1]Virginia Tech
[2]Space Science Institute
[3]Virginia Polytechnic Institute and State University
[4]British Antarctic Survey
[5]Department of Earth, Planetary, and Space Sciences

December 7, 2022

Abstract

On December 04, 2021, a total solar eclipse occurred over west Antarctica. Nearly an hour beforehand, a geomagnetic substorm onset was observed in the northern hemisphere. Eclipses are suggested to influence magnetosphere-ionosphere (MI) coupling dynamics by altering the conductivity structure of the ionosphere by reducing photoionization. This sudden and dramatic change in conductivity is not only likely to alter global MI coupling, but it may also introduce a variety of localized instabilities that appear in both hemispheres. Global navigation satellite system (GNSS) based observations of the total electron content (TEC) in the southern high latitude ionosphere during the December 2021 eclipse show signs of wave activity coincident with the eclipse peak totality. Ground magnetic observations in the same region show similar activity, and our analysis suggest that these observations are due to an "eclipse effect" rather than the prior substorm. We present the first multi-point interhemispheric study of a total south polar eclipse with local TEC observational context in support of this conclusion.

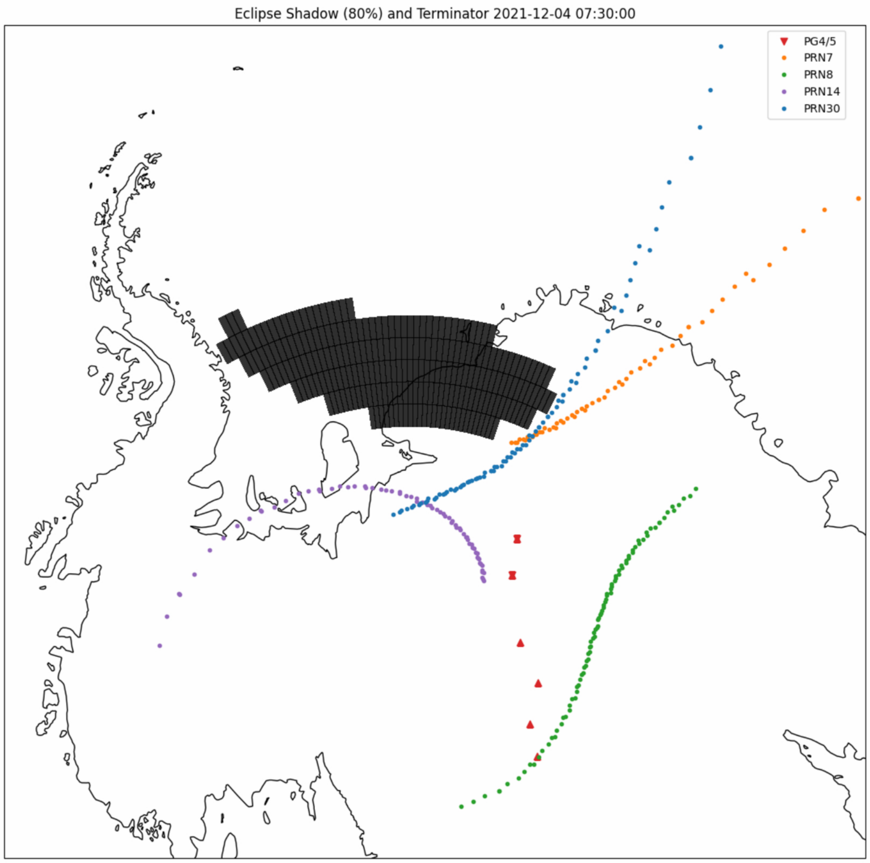
Eclipse Shadow (80%) and Terminator 2021-12-04 07:30:00
PG4/5
PRN7
PRN8
PRN14
PRN30

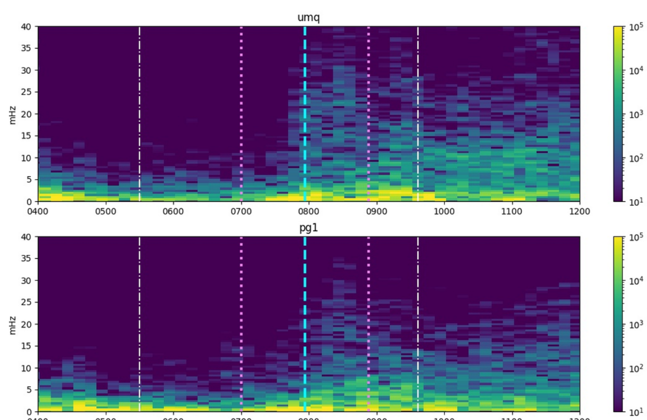
umq
pg1
mHz
nT^2Hz^{-1}
0400
0500
0600
0700
0800
0900
1000
1100
1200

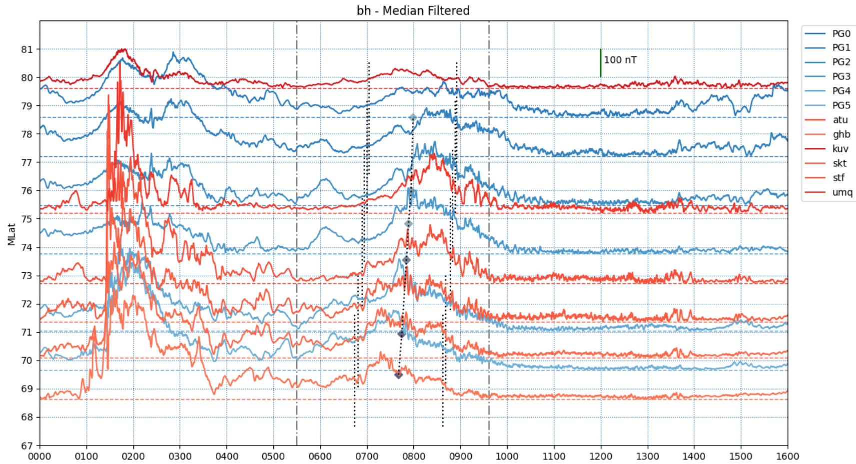

bh - Median Filtered
MLat
100 nT
PG0
PG1
PG2
PG3
PG4
PG5
atu
ghb
kuv
skt
stf
umq

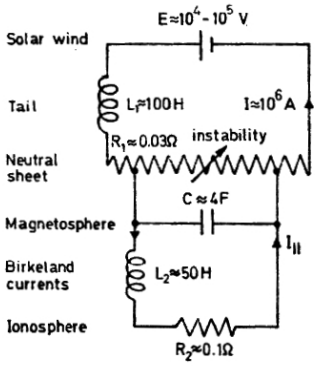

E≈10^4 - 10^5 V
Solar wind
Tail
L1≈100H
I≈10^6 A
R1≈0.03Ω
instability
Neutral sheet
C≈4F
Magnetosphere
Birkeland currents
L2≈50H
I∥
Ionosphere
R2≈0.1Ω

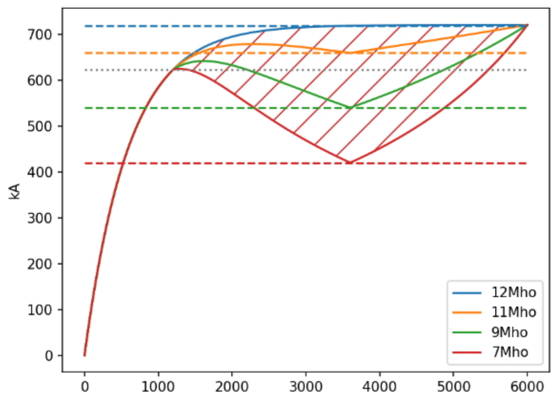

kA
12Mho
11Mho
9Mho
7Mho

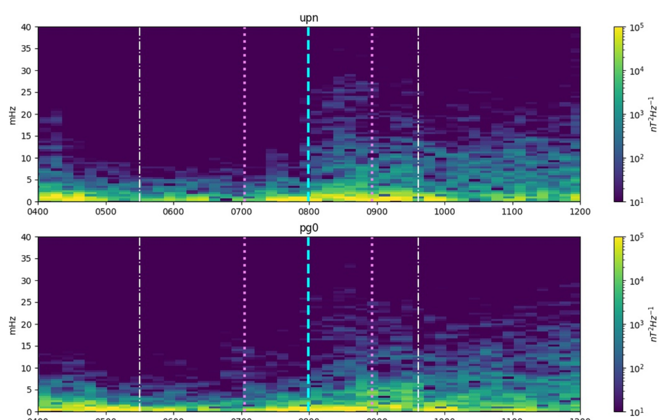

upn
pg0
mHz
nT²Hz⁻¹

The 2021 Antarctic Total Eclipse: Ground Magnetometer and GNSS Wave Observations from the 40 Degree Magnetic Meridian

S. E. Coyle[1], M. D. Hartinger[2,5], C. R. Clauer[1,3], J.B.H. Baker[1], I. Cnossen[4], M.P. Freeman[4], J.M. Weygand[5]

[1]Virginia Tech, Blacksburg, Virginia, USA
[2]Space Science Institute, Boulder, Colorado, USA
[3]National Institute of Aerospace, Hampton, Virginia, USA
[4]British Antarctic Survey, UK
[5]University of California, Los Angeles, California, USA

Key Points:

- A total solar eclipse occurred over Antarctica on December 4, 2021 alongside a geomagnetic substorm
- Variations in total electron content (TEC) are spatiotemporally correlated with eclipse shadow peak
- Similar ground magnetic variations are observed in both hemispheres, suggesting eclipse driven waves

Corresponding author: Shane Coyle, `shanec1@vt.edu`

Abstract

On December 04, 2021, a total solar eclipse occurred over west Antarctica. Nearly an hour beforehand, a geomagnetic substorm onset was observed in the northern hemisphere. Eclipses are suggested to influence magnetosphere-ionosphere (MI) coupling dynamics by altering the conductivity structure of the ionosphere by reducing photoionization. This sudden and dramatic change in conductivity is not only likely to alter global MI coupling, but it may also introduce a variety of localized instabilities that appear in both hemispheres. Global navigation satellite system (GNSS) based observations of the total electron content (TEC) in the southern high latitude ionosphere during the December 2021 eclipse show signs of wave activity coincident with the eclipse peak totality. Ground magnetic observations in the same region show similar activity, and our analysis suggest that these observations are due to an "eclipse effect" rather than the prior substorm. We present the first multi-point interhemispheric study of a total south polar eclipse with local TEC observational context in support of this conclusion.

Plain Language Summary

Solar eclipses occur when the Moon intersects the line between the Earth and the Sun. This configuration of Sun and Moon presents a unique opportunity to investigate the effects of the upper atmosphere's electrical conductivity on plasma waves that is independent of season or geomagnetic field orientation. We present observations of plasma waves in the high latitude region of Earth's upper atmosphere during the eclipse on December 04, 2021. These waves are similar to those else-wise observed near dawn in regions where the magnetic field lines connect to dark skies in one hemisphere and sunlit skies in the other. We suggest that the waves observed during the December 2021 eclipse have a similar generation mechanism to those that occur near dawn, a result of the difference in conductivities between magnetic field-line footprints.

1 Introduction

Solar eclipses provide an opportunity to study ionospheric dynamics in a way unlike any other. The majority of the sun's direct energy link into Earth's atmosphere is rapidly turned off and on again, and the impact of such a modulation is profound. Anyone who has experienced an eclipse from under the track of totality in person can attest to the dramatic temperature swings that occur from the momentary absence of sunlight. From the perspective of the global atmospheric system, the effects are equally noteworthy. Not only does an eclipse directly affect the thermosphere (McInerney et al., 2018; Li et al., 2021), but the obscuration related reduction in photoionization undoubtedly impacts the ionospheric composition (and therefore dynamics) as well (X. Chen et al., 2021; Dang et al., 2018). As a result of changes to the ionosphere's local total electron content (TEC), currents flowing within the ionosphere should also be modified by an eclipse. However, the exact physical description of how these currents are modified is an unsettled question, particularly in polar regions where data coverage is sparse and eclipses are relatively rare. It is therefore necessary for multi-point observations supported by modelling efforts to advance our understanding of eclipse related effects.

Several studies have suggested that ionosphere-thermosphere (IT) dynamics will be altered during an eclipse. One of the main drivers of these modified dynamics (at least at mid to low latitudes) is expected to be changes in the neutral wind structure that create counteracting flows in opposition to the regular wind dynamo (Aa et al., 2020; Choudhary et al., 2011; St.-Maurice et al., 2011). Because of coupling between the ionosphere and thermosphere, the normal evolution of the ionospheric electrojets are likely to be impacted as well by deviations in neutral winds. Couple this again with the well known reduction in photoionization that results from the lunar umbra, and a significant change in local ionospheric currents is the inevitable result.

An important facet of this modification of ionospheric currents is how this seemingly localized process can affect the global current systems. Because both ionospheres in the northern and southern hemispheres are magnetically coupled via the geomagnetic field, it follows that a changing current system in one may affect the other. Indeed, modelling efforts by Le et al. (2020) and X. Chen et al. (2021) as well as work by Zhang et al. (2020) show that variations in electron density and temperature at a particular point in one hemisphere can also impact the conjugate point in the other hemisphere. Regardless of hemisphere, these eclipse-induced changes in ionospheric electron density are known to have measurable impacts on human technology by affecting radio wave propagation (Moses et al., 2021; Frissell et al., 2018), and are therefore worth further investigation.

Despite having a long history of study (Stening et al., 1971), ground based magnetic observations from previous eclipses have presented an inconclusive picture of the expected response to the moon's passing. Momani et al. (2011) reported on the previous Antarctic total solar eclipse in 2003, showing a variation in the north-south component coincident with the eclipse signifying a change in the auroral electrojet overhead. Ladynin et al. (2011) presented a change in the north-south component from an eclipse in 2008. However, neither they nor Korte et al. (2001) could present an clearly identifiable response to the August 1999 eclipse. One reason for this discrepancy may have been the creation of hemispherically asymmetric current systems (Korte et al., 2001). Indeed, there are likely many factors at play that determine how much and in what ways an eclipse will impact ionospheric dynamics (and the corresponding magnetic signature), as suggested by Stankov et al. (2017) and Verhulst and Stankov (2020).

One of the unique features of this study is the investigation of wave-like structures that are apparently associated with the eclipse totality. These waves, as observed by ground-based magnetometers, fall into the ultra-low frequency (ULF) classification as in Jacobs et al. (1964). Many studies have been conducted on the properties of ULF waves at high latitudes (Simms et al., 2006; Martines-Bedenko et al., 2018; V. Pilipenko et al., 2015; V. A. Pilipenko et al., 2019; Constantinescu et al., 2009) in order to characterize their behavior. Furthermore, much has been published on the mechanisms that drive ULF waves in the magnetosphere (Anderson, 1993; Turc et al., 2022; Takahashi et al., 2021). However, because the eclipse's most notable feature is an absence of ionospheric photoionization, eclipses provide a unique opportunity to study less well documented ULF wave driving conditions.

The particular eclipse occurring on December 4, 2021 is rare in that it occurred at the high southern latitudes where total eclipses are often separated by nearly 20 years. While this is not the first time observations were made of an eclipse occurring over Antarctica, previous studies relied on a limited number of observing stations. This study is the first to utilize a large meridional array of magnetically conjugate instrument platforms in both hemispheres to provide magnetic observations in unprecedented detail. It is also the first to provide local TEC observations from the East Antarctic plateau as context for the magnetic variations.

2 Methodology

The focus of this study is to present observations of phenomena associated with the eclipse and coincident substorm from the vantage point of an array of instruments located along the 40 degree magnetic meridian in both Antarctica and Greenland. A comparison of models with and without an eclipse is conducted to give context on the expected response in TEC. This is then qualitatively compared to the raw line-of-sight (sometimes called "slant") TEC observations from Antarctica to confirm expected modification of ionospheric conductivity. Trends in TEC before and after the local eclipse totality are identified on a satellite by satellite basis. The most dramatic impacts are expected to occur at low elevations looking in the direction of the totality, thereby sensing the largest portion of the ionosphere covered by the shadow. Raw slant TEC data is shown with model TEC integrated along the ray path from ground to space. Additionally, spectrograms are also generated from the raw TEC measurements.

The other unique facet of this observational campaign stems from magnetometer measurements in both hemispheres. Short-time Fourier transform (STFT) spectrograms are created for each of the magnetically conjugate station pairs and an analysis of activity during the local eclipse window is conducted. Additionally, search-coil magnetometer measurements from the southern hemisphere stations are reviewed to provide additional context. These observations are then compared to nearby TEC measurements to draw conclusions about the source of any activity therein.

2.1 Ionosphere Modeling

The effects of the solar eclipse were simulated with the Thermosphere-Ionosphere-Electrodynamics General Circulation Model (TIE-GCM) version 2.0 (Richmond et al., 1992; Qian et al., 2014). Simulations were performed with a 2.5 degree horizontal grid spacing and a vertical resolution of 1/4 scale height, with vertical levels ranging from about 97 to 500 km altitude. Observed solar wind and interplanetary magnetic field data were used to drive the auroral parameterization and the Weimer (2005b) high-latitude electric field model. Instantaneous and 81-day average F10.7 data were used to characterize the solar extreme ultraviolet (EUV) radiative forcing. Output data were stored every 15 minutes from 0 UT on 4 December 2021 until 0 UT on 6 December 2021, although we just use hourly outputs from 0530 UT until 0830 UT here. For the purposes of exploring the eclipse effect, the baseline model run was compared to an "eclipse" run with an imposed shadow. For the "eclipse" simulation, location-dependent solar obscuration factors were calculated with the Python package provided by Verhulst and Stankov (2020). Separate obscuration factors were calculated for the visible and EUV parts of the spectrum, taking into account that EUV emissions from the solar corona are not fully blocked, as recommended by Verhulst and Stankov (2020). Both simulations were initialized from a 30-day spin-up simulation to allow the model to reach a quasi-steady state.

In an attempt to better understand the connection between the substorm related effects and eclipse effects, we utilize a well-established empirical model for solar wind-magnetosphere coupling. While sensing the interplanetary magnetic field (IMF) directly (as in via the OMNI database) is certainly useful in this effort, the relationship between the IMF and ionospheric currents is complex. A useful model to estimate ionospheric driving from solar wind data was developed by Weimer in the mid 90s and has since then been refined (Weimer, 1995, 2005a, 2005b). This model provides an estimate of the cross polar cap potential (CPCP), which maps to the ionosphere the electric potential imposed on the magnetotail by the solar wind convection. We use this model to both provide context for the state of the electric field throughout the ionosphere, as well as to provide an estimate of the energy contained in the disruption created by the eclipse.

2.2 GPS TEC Observations

Thanks to a coordinated effort to observe the 2021 Antarctic eclipse in unprecedented detail, high cadence (10s) TEC observations are available during a several day window around the eclipse. Contributions from glaciology researchers and global navigation satellite system (GNSS) receivers as part of the The Polar Earth Observing Network (POLENET), Antarctic Network (A-NET), and United Kingdom Antarctic Network (UKANET) were leveraged to make up for an otherwise sparsely sampled region of West Antarctica. On the East Antarctic plateau, the Autonomous Adaptive Low-Power Instrument Platforms (AAL-PIPs, Figure 1) provide both critical GNSS-derived TEC measurements as well as ground magnetic observations. Due to hardware limitations at the AAL-PIP sites, only a single site could collect TEC observations at any one time (ex-

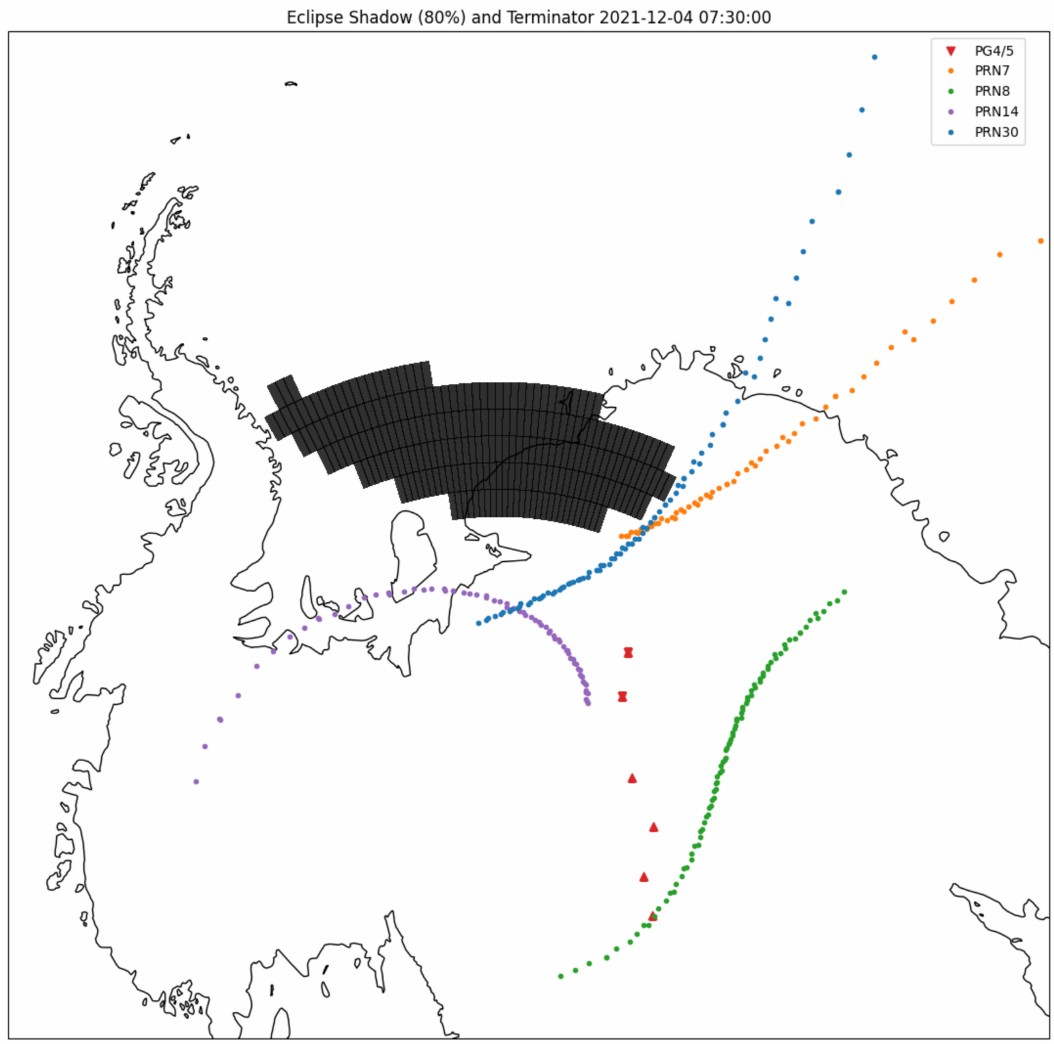

Figure 1. Map of Antarctica showing the location of the eclipse shadow defined by an obscuration of 80% around the time of peak totality (0730 UT). The shaded region moves nominally from top to bottom over the course of the eclipse period (roughly 4hr). AAL-PIP sites are plotted as red triangles, with PG4/5 overplotted with downward triangles. Ray paths for select GNSS satellites are traced to an altitude of 600km for the duration of their respective measurements and organized by color. The sun is to the right of the figure, the solar terminator is to the left.

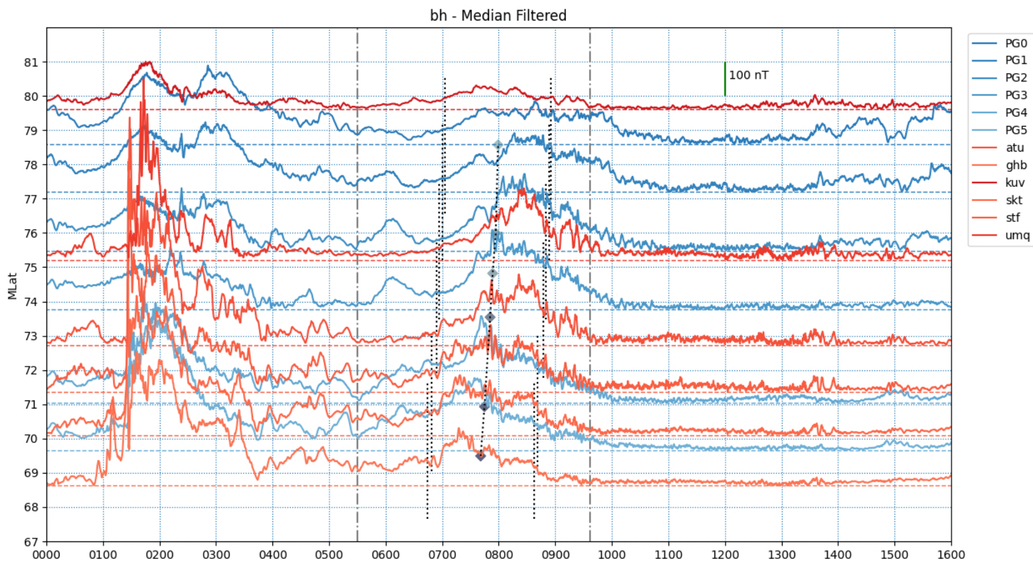

Figure 2. Horizontal component of the magnetic field variations organized by magnetic latitude, with 1 degree scaled to represent 100 nT. The six southern (northern) hemisphere stations are in blue (red). Dot-dashed lines represent the entire eclipse interval, while short dashed lines represent the local shadow interval. Diamonds represent the progression of the peak obscuration point across the array. An earlier substorm occurs between 1-2 UT, with a much smaller substorm occurring between 6-7 UT.

cepting a few minutes of overlap). Thus, we treat the entire array as a single mesoscale observation platform for the purpose of TEC measurements. To provide as great a temporal resolution as possible the cadence of these measurements was set to every $10s$. Observations are unique to each satellite, and are uniquely identified by a pseudo-random number (PRN) code. These measurements are then compared to TEC integrated along similar rays traced through the TIE-GCM model ionosphere.

2.3 Magnetometer Observations

The AAL-PIPs are a series of 6 ground-based observation platforms located along the 40° magnetic meridian between 69 and 79 degrees latitude (Clauer et al., 2014). Each station has an approximately magnetically conjugate counterpart on the west coast of Greenland operated by the Danish Technical University. Combining observations from both arrays provides a unique perspective on the global magnetospheric system and any interhemispheric asymmetries that may occur. Both arrays operate fluxgate magnetometers at each site, while the AAL-PIP array also operates search-coil magnetometers and the previously mentioned GNSS receivers at 4 of 6 sites.

In order to identify substorm occurrence, we utilize the auroral electrojet (AE) index provided by the World Data Center hosted by Kyoto University (Iyemori et al., 1992). The AE index is a composite of the horizontal deviation of the magnetic field at a dozen locations in the auroral region, which give a sense of the strength of the ionospheric currents flowing overhead. These currents are enhanced during periods of increased geomagnetic activity, such as during substorms. It is also possible to identify substorm signatures in ground magnetometer observations directly as shown in the AAL-PIP and DTU time-series (Figure 2).

3 Analysis and Results

3.1 TEC

Figure 3 shows slant TEC traced from the ground to select satellites in the control model (orange), eclipse model (green), and observation (blue). The local totality window (0648-0841 UT), the local totality peak (0744 UT), and the global totality peak (0733 UT) are all marked by vertical dashed and dotted lines. Figure 4 shows the spectrogram representation of the TEC observations, also with vertical lines representing the local totality window and peak. The largest difference observed between the model observations is approximately 4 TECU at the time of the local peak totality. Similar reductions in the Hall and Pedersen in the height integrated conductivities are apparent in the eclipse model runs compared to the control. Observations of slant TEC from AAL-PIP are moderately in agreement with the models, with a few exceptions. A sharp increase in the TEC observations appears in PRNs 8 and 30 around the time of the global totality peak. TEC along the path to PRN 14 does appear to have any clear eclipse related signature, while after the peak obscuration PRNs 8, 30, and 7 begin to increase at varying rates. This is in contrast to the expectations put forth by the model, which suggest a much slower recovery from the eclipse. Moreover, the TEC observed by PG4/5 has a step-function-like increase after the global eclipse peak, indicating that TEC has increased beyond pre-eclipse levels. There also appears to be a general increase in ULF wave activity coincident with the local time of the global peak obscuration, preceded by some higher frequency activity in the 40-50 mHz range. This is most apparent in the spectrogram of PRNs 8 and 30 in Figure 4.

3.2 Magnetic Variations

The horizontal magnetic variation shown in Figure 2 is defined as the magnitude of the sum of the median filtered data to eliminate any bias from the DC magnetic field:

$$B_h = \sqrt{(B_x - \tilde{B_x})^2 + (B_y - \tilde{B_y})^2} \tag{1}$$

where B_x, B_y are the north/south and east/west aligned components of the magnetic field measurement, and $\tilde{B_x}, \tilde{B_y}$ are the median values of those components. The horizontal variation plot shows an easily identifiable substorm occurring just prior to 02 UT. Additionally, there is activity occurring in both hemispheres near 0630. This small increase in magnetic activity occurs first in the southern hemisphere, and then in the northern hemisphere. Shortly after 0640, another disturbance occurs nearly simultaneously in both hemispheres, first at low latitudes and then at higher latitudes (7-9 UT). This activity is well correlated to the time period when the eclipse shadow is present at each of the stations in the southern array. After the eclipse period is over, the remainder of the day is comparatively uneventful from the perspective of the magnetometer data. Analysis of the spectral composition of the fluxgate magnetometer (Figure 5, Supplemental Figure S1-S4) data shows an increase in ultra-low frequency (ULF) waves in the $20-40mHz$ band that is tightly bounded by the occurrence of the local peak obscuration at each station. These waves fall into the pulsation continuous 3 (PC3) band based on the common ULF wave schema (Jacobs et al., 1964). A similar signature is observed in the search-coil spectrograms (Figure 6, Supplemental Figure S5-S7) at each station where they're available. There is a slight enhancement in wave activity around 0640 UT that is more apparent in the search-coil data because of its higher sampling rate. This activity may be indicative of the substorm observed in the AE index and subsides just prior to the local eclipse interval. It is also worth noting that the wave power increase observed in the magnetometer measurements is in a similar frequency band to that observed in the TEC data. Additionally, Figure 6 shows an apparent suppression of wave activity above 0.2 Hz.

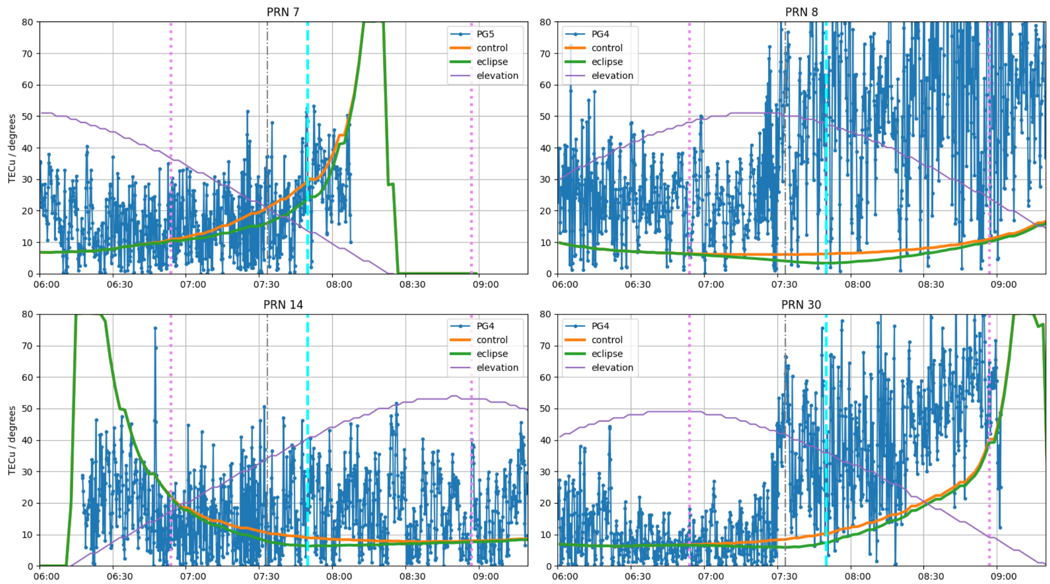

Figure 3. Line of sight TEC as measured from PG4/PG5. Elevation angle is plotted in magneta. TEC integrated along the ray path through TIE-GCM model ionosphere are plotted in orange (control) and green (eclipse). Blue lines are 10s TEC samples for each of the selected GNSS satellites (identified by their respective PRN). Vertical lines at 0654, 0733, 0750, and 0857 UT indicate the local eclipse start, global peak, local peak, and local eclipse end. PRN 7 shows fairly good agreement between model and observations as the elevation angle decreases. PRNs 8 & 30 show a significant increase in TEC occurring shortly after the global totality peak. PRN 14 shows very little activity associated with the eclipse, which may be due to the geometry of the ray path to that particular satellite.

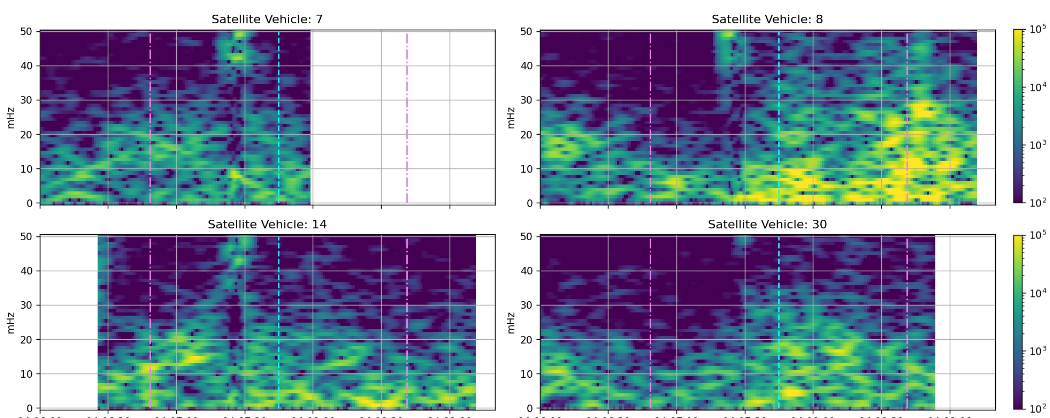

Figure 4. Spectral components of TEC measurements in Figure 3. Note the sharp increase in wave power near the local peak in obscuration in PRNs 8 & 30. All PRNs show an increase in wave power around 50 mHz just prior to the global totality peak.

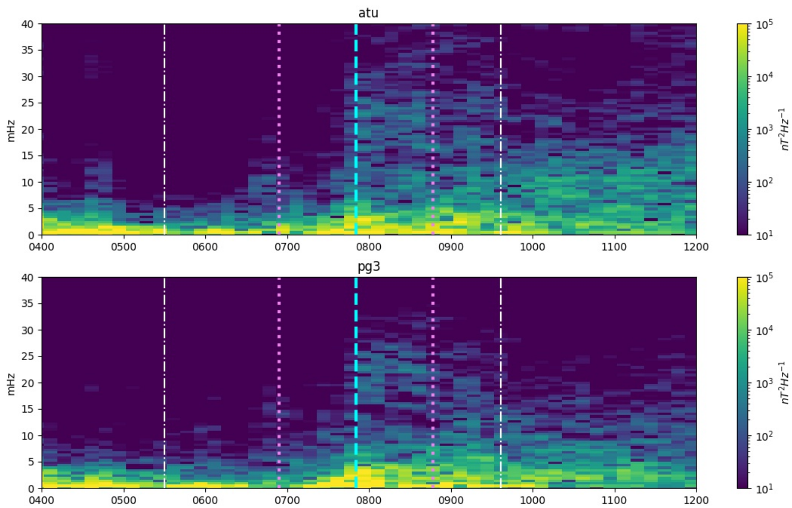

Figure 5. Spectrogram of fluxgate magnetometer data from ATU in Greenland and the conjugate station PG3 in Antarctica. White dot-dashed lines indicate the time interval of the entire eclipse (eclipse contact points P1 & P4), while the magenta dotted lines indicate the local eclipse interval at PG3. The cyan dashed line in the middle indicates the time of localized peak obscuration, which coincides with an increase in activity near 20 mHz.

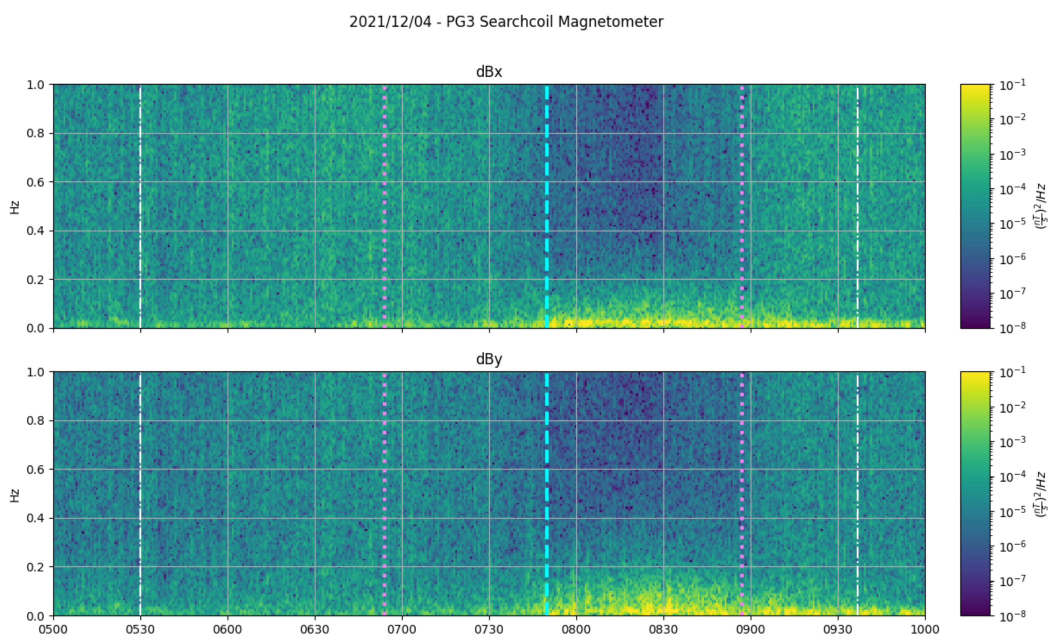

Figure 6. Search-coil magnetometer spectrogram, also from PG3. Similar temporal coincidence of waves and local obscuration peak is observed, though with a higher dynamic range of frequencies. A possible signature of the 0640 UT substorm is observed and subsides prior to the local onset of PC3 waves.

4 Discussion

It is expected that during an eclipse, one would experience a localized reduction in TEC leading up to the peak obscuration followed by an increase in TEC as the solar disk re-emerges. This is well illustrated in the difference between control and eclipse event model TEC outputs show in Figure 3. It is noted that while deviations of on the order of 40 TEC units may seem quite large, line of sight measurements at low elevation angles are sensing a much larger portion of the ionospheric layers than the more common vertical TEC measurements. Idosa and Rikitu (2022) show similar modification of TEC upwards of 14 TEC units under the region of shadow for the same event. One question about the observations from PG4/5 remains outstanding: Why is there a step-function-like increase in TEC immediately after the global peak obscuration, specifically in PRN 8 and 30 but not otherwise? This is not the first time such an observation has been made during an eclipse (G. Chen et al., 2013; Cherniak & Zakharenkova, 2018; Wu et al., 2018). A simple explanation for why the observations differ at all can be attributed to the geometry of the ray paths and specifically the azimuth of the satellites from the ground. If these differences are indeed indicative of a localized increase in TEC, one possible explanation may be auroral precipitation. This mechanism would explain both the spatial dependence as well as the apparent increase in TEC beyond "pre-eclipse" levels. While it is well known that auroral activity increases during geomagnetic substorms, further investigation by way of satellite observation and modeling may help determine the feasibility of a direct eclipse effect on precipitation. Another possible explanation for the post-eclipse enhancement was suggested in Cnossen et al. (2019) which relies on strong vertical drifts storing plasma at high altitudes and reversing after the eclipse. Again, direct observation of the plasma motion either by ground or space based instrumentation would aid in our understanding of this phenomenon.

Determining if and how the eclipse impact on the ionosphere modifies the currents flowing within is a non-trivial task. It is therefore potentially useful to represent the coupled solar wind-magnetosphere-ionosphere (SWMI) using a circuit model as in Boström (1974). The ionosphere in this model is typically represented as a load on the magnetosphere coupled by field aligned currents. It is reasonable to expect that by modifying the ionospheric resistance, the resultant currents are similarly modified. If one holds the magnetospheric potential to be constant, the ionospheric portion of the circuit can be reduced to a series inductor-resistor (LR) configuration with some ionospheric potential like that from Weimer (1995). An example current profile generated by varying the resistance of the ionosphere is shown in Figure 7. Interestingly, a simple integration of the energy "diverted" from the ionosphere in this manner over the period of an eclipse is of similar magnitude to what has been suggested is sufficient to drive the magnetotail to instability (Akasofu, 2021). For a CPCP at $60kV$, $L_{FAC} = 50H$, and $t_{eclipse} \approx 4hrs$:

$$E_{diverted} = CPCP \cdot \int I_{iono} - I_{eclipse}\, dt \approx 2 \times 10^{14} J \tag{2}$$

It is possible that a reduction in current passing through the ionosphere contributes to currents flowing elsewhere in the magnetosphere, but it is also possible (and perhaps more likely) that the magnetospheric potential driving these currents is not constant. Clearly any conclusions about energy flux must necessarily provide more sophisticated modelling support than what is provided here.

Previous studies have shown a propensity for substorm activity to occur preferentially in dark hemispheres (lower conductivity) compared to sunlit (Laundal et al., 2017; Liou et al., 2018; Singh et al., 2011; Wang et al., 2005; Wang & Lühr, 2007). It is difficult, however, to separate out other seasonal effects like the Russell-McPheron effect (Russell & McPherron, 1973) or thermospheric effects. Eclipses provide a unique opportunity to study how substorm characteristics can be altered by changes in conductivity independent of season. Interestingly, this is not the first time enhanced geomagnetic activity has been observed concurrently with a solar eclipse (Cherniakov, 2017; Rashid et

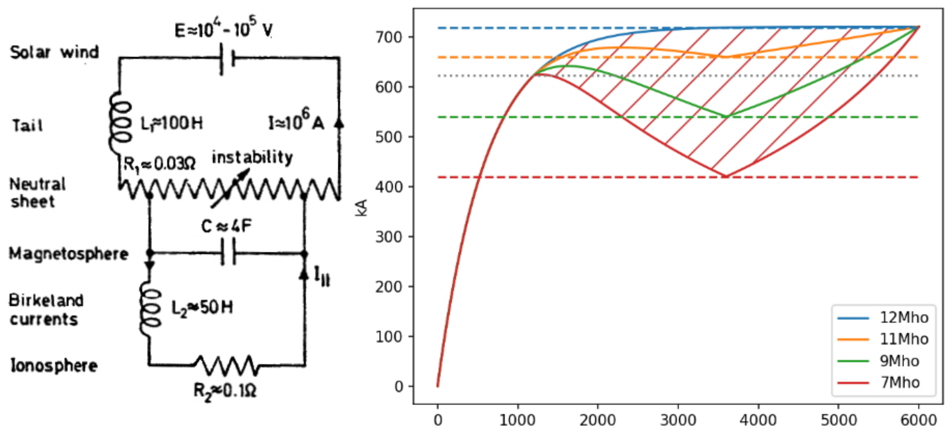

Figure 7. Circuit schematic of the SWMI system as in Boström (1974). During an eclipse, the ionospheric load changes rapidly and acts more like a variable resistance. An example current profile of the series LR circuit representing magnetosphere-ionosphere currents is given for $V_{PC} = 60kV$ (from Weimer), $L_{FAC} = 50H$ and $R_{iono} = 12^{-1}\Omega$. The resistance value is varied linearly from $12^{-1}\Omega$ to $7^{-1}\Omega$ for a time to simulate an eclipse. The area between the curves represents a difference in energy dissipation through the ionosphere because of the reduced conductivity.

al., 2006). It is therefore suggested that a followup study be conducted in order to identify any particular linkages between eclipses, substorms, and/or ionospheric current systems in general, with the overarching goal to better understand the impact of conductivity on the magnetosphere-ionosphere coupling system.

The eclipse is associated with large spatiotemporal variations in TEC, and subsequently in both Hall and Pedersen conductivities. Newton et al. (1978) illustrates how conductivity is related to ULF wave dissipation. Likewise, Allan and Knox (1979); Allan (1982) discuss the impact of interhemispheric asymmetries in conductivity on magnetospheric waves. It is therefore well within reason to suggest that rapid variation of conductivity in one hemisphere (like during an eclipse) is likely to alter wave properties along the magnetic field line linking the hemispheres. It is suggested in Allan (1983) that "quarter-wave" pulsations occur in regions where the ionospheric conductivity at the magnetic foot-points is highly asymmetric, and Obana et al. (2015) presents observations of such waves, as well as a phase transition from "quarter-wave" mode to "half-wave" mode associated with the dawnside terminator. Similar interhemispheric conductivity ratios to Figure 15 of Obana et al. (2015) are predicted by the TIE-GCM eclipse model for this event, suggesting these waves may have a similar generation mechanism.

Recent work investigating the occurrence of PC3 waves at the dawnside terminator has shown evidence of what is termed the "sunrise effect" (Saka & Alperovich, 1993; Somsikov, 2011; Tanaka et al., 2004; Yagova et al., 2017; Silva et al., 2020). While the physical processes underlying the generation of these waves remains poorly understood, it is noteworthy that PC3 waves occur frequently at the dawn side terminator. It is then perhaps no coincidence that PC3 waves are observed by the AAL-PIP and DTU magnetometers during the December 2021 eclipse, as this is liken to a "second sunrise" where photoionization is suddenly reintroduced into a darkened ionosphere. However, most observations of the "sunrise effect" have been at mid to low latitudes, where ionospheric currents behave quite differently than at the high latitudes studied herein. One of the proposed generation mechanisms for these waves involves the motion of neutral winds across a thermal conductivity gradient (Silva et al., 2020). It is therefore suggested that further observational study of eclipse related ULF waves include a thermospheric wind measurement in conjunction with ionospheric sounding.

It may be tempting to associate the occurrence of ULF waves with well known magnetospheric drivers like upstream pressure variations from the solar wind or ion foreshock (Anderson, 1993; Turc et al., 2022; Takahashi et al., 2021). Indeed, this may explain why longer period PC5 waves are being driven as well (Hartinger et al., 2013). There are two reasons why these observations do not support such a mechanism. First, the difference in wave onset times between the most pole-ward and equator-ward stations is nearly 20 minutes, much longer than would be expected. Secondly, the waves occur first at the more equatorial station before moving pole-ward. The wave activity is also inconsistent with internally driven waves which tend to have wave power concentrated in a much narrower range of latitudes than that shown in Figure 2 (Shi et al., 2018). Though internal or external drivers may be supplying some energy to sustain the waves, the eclipse-related IT system changes are the primary factors controlling wave activity during this period.

This study is not the first time ground magnetic observations of waves in proximity to an eclipse have been reported. Kim and Chang (2018) utilize wavelet analysis to identify the frequency specific response to several total solar eclipses in comparison to a similar time period 24 hrs later. They describe an eclipse related suppression of wave activity at frequencies well above the PC3 range. Indeed, the search-coil spectrum of Figure 6 does show an apparent damping of wave activity in the upper portion of the figure after the totality peak. This suggests there is a frequency dependence on the impact of the eclipse on ionospheric dynamics.

4.1 Summary and Conclusions

We have presented observations of a total solar eclipse occurring over Antarctica on 04 December, 2021. In summary:

- Just prior to peak totality (0730 UT), a substorm (0640 UT) was observed in the AE index as well as in the combined 40 degree array magnetograms
- TIE-GCM model runs predict peak reduction in slant total electron content of around 4 TECU during an eclipse
- Line-of-sight TEC observations near the path of totality show an increase in TEC after the peak totality for some regions of the ionosphere
- Magnetic oscillations in the PC3 band occur coincident with the local peak obscuration at several ground magnetometer stations in both north and south hemispheres.
- TEC oscillations are observed to be of similar frequency to those observed in magnetometer data
- It appears that these oscillations occur independent of the substorm occurring during the eclipse, but more investigation is required to explain the physical processes involved
- Subsequent studies of eclipses would greatly benefit from advanced diagnostics of the neutral atmosphere and ionospheric dynamics
- Coordinated, multi-point observations are required to "close the loop" on the ionospheric eclipse effect

v

5 Open Research

GNSS data used in this study is available at `mist.nianet.org`, via MADRIGAL (`http://cedar.openmadrigal.org/`) or by request. Magnetometer data from DTU can be obtained via the Tromsø Geophysical Observatory (`https://flux.phys.uit.no/geomag.html`). Southern hemisphere magnetometer data is available via `mist.nianet.org`. The AE index is available at `https://wdc.kugi.kyoto-u.ac.jp/ae_realtime/202112/index_20211204.html`. GNSS satellite position data can be obtained via `https://in-the-sky.org/satmap_globe.php?year=2021&month=12&day=4`. Eclipse details are available via `https://eclipse.gsfc.nasa.gov/`. The TIE-GCM model is available at `https://www.hao.ucar.edu/modeling/tgcm/tie.php`.

Acknowledgments

S.E. Coyle was supported by the Virginia Tech ECE Bradley Department as well as NSF grants 1543364 and 2027168. C.R. Clauer was supported by NSF grant 1543364 and 1744828. M.D. Hartinger was supported by NSF grant AGS-2027210. J.B. Baker was supported by NSF grant 2027168. I. Cnossen was supported by a Natural Environment Research Council (NERC) Independent Research Fellowship (NE/R015651/1).

References

Aa, E., Zhang, S.-R., Erickson, P. J., Goncharenko, L. P., Coster, A. J., Jonah, O. F., ... Liu, L. (2020). Coordinated ground-based and space-borne observations of ionospheric response to the annular solar eclipse on 26 december 2019. *Journal of Geophysical Research: Space Physics*, *125*(11), e2020JA028296.

Akasofu, S.-I. (2021). A review of studies of geomagnetic storms and auroral/magnetospheric substorms based on the electric current approach. *Frontiers in Astronomy and Space Sciences*, 100.

Allan, W. (1982). Phase variation of ulf pulsations along the geomagnetic field-line. *Planetary and Space Science*, *30*(4), 339–346.

Allan, W. (1983). Quarter-wave ulf pulsations. *Planetary and Space Science*, *31*(3), 323–330.

Allan, W., & Knox, F. (1979). The effect of finite ionosphere conductivities on axisymmetric toroidal alfvén wave resonances. *Planetary and Space Science*, *27*(7), 939–950.

Anderson, B. J. (1993). Statistical studies of pc 3-5 pulsations and their relevance for possible source mechanisms of ulf waves. In *Annales geophysicae* (Vol. 11, pp. 128–143).

Boström, R. (1974). Ionosphere-magnetosphere coupling. In *Magnetospheric physics* (pp. 45–59). Springer.

Chen, G., Qi, H., Ning, B., Zhao, Z., Yao, M., Deng, Z., ... others (2013). Night-time ionospheric enhancements induced by the occurrence of an evening solar eclipse. *Journal of Geophysical Research: Space Physics*, *118*(10), 6588–6596.

Chen, X., Dang, T., Zhang, B., Lotko, W., Pham, K., Wang, W., ... others (2021). Global effects of a polar solar eclipse on the coupled magnetosphere-ionosphere system. *Geophysical Research Letters*, *48*(23), e2021GL096471.

Cherniak, I., & Zakharenkova, I. (2018). Ionospheric total electron content response to the great american solar eclipse of 21 august 2017. *Geophysical Research Letters*, *45*(3), 1199–1208.

Cherniakov, S. (2017). Solar eclipses at high latitudes: ionospheric effects in the lower ionosphere. In *2017 fall meeting.*

Choudhary, R., St.-Maurice, J.-P., Ambili, K., Sunda, S., & Pathan, B. (2011). The impact of the january 15, 2010, annular solar eclipse on the equatorial and low latitude ionospheric densities. *Journal of Geophysical Research: Space Physics*, *116*(A9).

Clauer, C. R., Kim, H., Deshpande, K., Xu, Z., Weimer, D., Musko, S., … Ridley, A. J. (2014). An autonomous adaptive low-power instrument platform (aal-pip) for remote high-latitude geospace data collection. *Geoscientific Instrumentation, Methods and Data Systems*, *3*(2), 211–227. Retrieved from https://www.geosci-instrum-method-data-syst.net/3/211/2014/ doi: 10.5194/gi-3-211-2014

Cnossen, I., Ridley, A., Goncharenko, L., & Harding, B. (2019). The response of the ionosphere-thermosphere system to the 21 august 2017 solar eclipse. *Journal of Geophysical Research: Space Physics*, *124*(8), 7341–7355.

Constantinescu, O. D., Glassmeier, K.-H., Plaschke, F., Auster, U., Angelopoulos, V., Baumjohann, W., … Magnes, W. (2009, 01). Themis observations of duskside compressional pc5 waves. *J. Geophys. Res.*, *114*, n/a-n/a. Retrieved 2019-4-3, from 10.1029/2008ja013519 doi: 10.1029/2008ja013519

Dang, T., Lei, J., Wang, W., Zhang, B., Burns, A., Le, H., … Wan, W. (2018). Global responses of the coupled thermosphere and ionosphere system to the august 2017 great american solar eclipse. *Journal of Geophysical Research: Space Physics*, *123*(8), 7040–7050.

Frissell, N. A., Katz, J. D., Gunning, S. W., Vega, J. S., Gerrard, A. J., Earle, G. D., … others (2018). Modeling amateur radio soundings of the ionospheric response to the 2017 great american eclipse. *Geophysical Research Letters*, *45*(10), 4665–4674.

Hartinger, M., Turner, D., Plaschke, F., Angelopoulos, V., & Singer, H. (2013). The role of transient ion foreshock phenomena in driving pc5 ulf wave activity. *Journal of Geophysical Research: Space Physics*, *118*(1), 299–312.

Idosa, C. U., & Rikitu, K. S. (2022). Effects of total solar eclipse on ionospheric total electron content over antarctica on 2021 december 4. *The Astrophysical Journal*, *932*(1), 2.

Iyemori, T., Takeda, M., Nose, M., Toh, H., Odagi, Y., & Takeuchi, N. (1992). *Magnetic data at wdc kyoto—services under international collaborations.* Retrieved from https://wdc.kugi.kyoto-u.ac.jp/ae_realtime/202112/index_20211204.html

Jacobs, J. A., Kato, Y., Matsushita, S., & Troitskaya, V. A. (1964). Classification of geomagnetic micropulsations. *Journal of Geophysical Research (1896-1977)*, *69*(1), 180–181. Retrieved 2019-03-28, from https://agupubs.onlinelibrary.wiley.com/doi/abs/10.1029/JZ069i001p00180 doi: 10.1029/JZ069i001p00180

Kim, J.-H., & Chang, H.-Y. (2018). Geomagnetic field variations observed by intermagnet during 4 total solar eclipses. *Journal of Atmospheric and Solar-Terrestrial Physics*, *172*, 107–116.

Korte, M., Lühr, H., Förster, M., Haak, V., Bencze, P., et al. (2001). Did the solar eclipse of august 11, 1999, show a geomagnetic effect? *Journal of Geophysical Research: Space Physics*, *106*(A9), 18563–18575.

Ladynin, A., et al. (2011). Changes in the daily geomagnetic variation during the total solar eclipse of 1 august 2008. *Russian Geology and Geophysics*, *52*(3), 343–352.

Laundal, K. M., Cnossen, I., Milan, S. E., Haaland, S., Coxon, J., Pedatella, N., … Reistad, J. P. (2017). North–south asymmetries in earth's magnetic field. *Space Science Reviews*, *206*(1), 225–257.

Le, H., Liu, L., Ren, Z., Chen, Y., Zhang, H., et al. (2020). Effects of the 21 june 2020 solar eclipse on conjugate hemispheres: A modeling study. *Journal of Geophysical Research: Space Physics*, *125*(11), e2020JA028344.

Li, R., Lei, J., & Dang, T. (2021). The solar eclipse effects on the upper thermosphere. *Geophysical Research Letters*, *48*(15), e2021GL094749.

Liou, K., Sotirelis, T., & Mitchell, E. J. (2018). North-south asymmetry in the geographic location of auroral substorms correlated with ionospheric effects. *Sci-*

entific reports, *8*(1), 1–6.

Martines-Bedenko, V., Pilipenko, V., Hartinger, M., Engebretson, M., Lorentzen, D., & Willer, A. (2018). Correspondence between the latitudinal ulf wave power distribution and auroral oval in conjugate ionospheres. *Sun and Geosphere*. Retrieved 2019-4-3, from `10.31401/sungeo.2018.01.06` doi: 10.31401/sungeo.2018.01.06

McInerney, J. M., Marsh, D. R., Liu, H.-L., Solomon, S. C., Conley, A. J., & Drob, D. P. (2018). Simulation of the 21 august 2017 solar eclipse using the whole atmosphere community climate model-extended. *Geophysical Research Letters*, *45*(9), 3793–3800.

Momani, M., et al. (2011). Magnetic field disturbances during the 2003 total solar eclipse over antarctica as observed by magnetometers. *Eur. J. Technol. Adv. Eng. Res.*, *2*, 69–75.

Moses, M., Kordella, L., Earle, G., Drob, D., Huba, J., Ruohoniemi, J., … Sivakumar, V. (2021). Observations and modeling studies of solar eclipse effects on oblique high frequency radio propagation. *Space Weather*, *19*(3), e2020SW002560.

Newton, R., Southwood, D., & Hughes, W. (1978). Damping of geomagnetic pulsations by the ionosphere. *Planetary and Space Science*, *26*(3), 201–209.

Obana, Y., Waters, C. L., Sciffer, M. D., Menk, F. W., Lysak, R. L., Shiokawa, K., … Petersen, T. (2015). Resonance structure and mode transition of quarter-wave ulf pulsations around the dawn terminator. *Journal of Geophysical Research: Space Physics*, *120*(6), 4194–4212.

Pilipenko, V., Belakhovsky, V., Engebretson, M., Kozlovsky, A., & Yeoman, T. (2015, 03). Are dayside long-period pulsations related to the cusp? *Annales Geophysicae*, *33*, 395-404. doi: 10.5194/angeo-33-395-2015

Pilipenko, V. A., Fedorov, E. N., Hartinger, M. D., & Engebretson, M. J. (2019). Electromagnetic fields of magnetospheric ulf disturbances in the ionosphere: Current/voltage dichotomy. *Journal of Geophysical Research: Space Physics*, *124*(1), 109–121. doi: 10.1029/2018ja026030

Qian, L., Burns, A., Emery, B., Foster, B., Lu, G., & Maute, A. (2014). & wang, w. *The NCAR TIE-GCM: A community model of the coupled thermosphere/ionosphere system. Modeling the ionosphere-thermosphere system*, *201*, 73–83.

Rashid, Z. A. A., Momani, M. A., Sulaiman, S., Ali, M. A. M., Yatim, B., Fraser, G., & Sato, N. (2006). Gps ionospheric tec measurement during the 23rd november 2003 total solar eclipse at scott base antarctica. *Journal of Atmospheric and Solar-Terrestrial Physics*, *68*(11), 1219–1236.

Richmond, A., Ridley, E., & Roble, R. (1992). A thermosphere/ionosphere general circulation model with coupled electrodynamics. *Geophysical Research Letters*, *19*(6), 601–604.

Russell, C., & McPherron, R. (1973). Semiannual variation of geomagnetic activity. *Journal of geophysical research*, *78*(1), 92–108.

Saka, O., & Alperovich, L. (1993). Sunrise effect on dayside pc pulsations at the dip equator. *Journal of Geophysical Research: Space Physics*, *98*(A8), 13779–13786.

Shi, X., Baker, J., Ruohoniemi, J., Hartinger, M., Murphy, K., Rodriguez, J., … Angelopoulos, V. (2018). Long-lasting poloidal ulf waves observed by multiple satellites and high-latitude superdarn radars. *Journal of Geophysical Research: Space Physics*, *123*(10), 8422–8438.

Silva, G. B., Padilha, A. L., & Alves, L. R. (2020). Latitudinal variation of pc3–pc5 geomagnetic pulsation amplitude across the dip equator in central south america. In *Annales geophysicae* (Vol. 38, pp. 35–49).

Simms, L. E., Engebretson, M. J., Posch, J. L., & Hughes, W. J. (2006). Effects of the equatorward auroral boundary location and solar wind parameters on pc5 activity at auroral zone stations: A multiple regression analysis. *J. Geophys. Res.*, *111*. Retrieved 2019-4-3, from 10.1029/2005ja011587 doi: 10.1029/2005ja011587

Singh, A. K., Jayashree, B., Sinha, A. K., Rawat, R., Pathan, B., & Dhar, A. (2011). Observations of near-conjugate high-latitude substorms and their low-latitude implications. *Current Science*, 1073–1078.

Somsikov, V. (2011). Solar terminator and dynamic phenomena in the atmosphere: A review. *Geomagnetism and Aeronomy*, *51*(6), 707–719.

Stankov, S. M., Bergeot, N., Berghmans, D., Bolsée, D., Bruyninx, C., Chevalier, J.-M., ... others (2017). Multi-instrument observations of the solar eclipse on 20 march 2015 and its effects on the ionosphere over belgium and europe. *Journal of Space Weather and Space Climate*, *7*, A19.

Stening, R., Gupta, J., & Van Beek, G. J. (1971). Magnetic observations in canada during the solar eclipse of march 7, 1970. *Nature (Phys. Sci.)*, *230*, 22–23.

St.-Maurice, J.-P., Ambili, K., & Choudhary, R. (2011). Local electrodynamics of a solar eclipse at the magnetic equator in the early afternoon hours. *Geophysical Research Letters*, *38*(4).

Takahashi, K., Turc, L., Kilpua, E., Takahashi, N., Dimmock, A., Kajdic, P., ... others (2021). Propagation of ultralow-frequency waves from the ion foreshock into the magnetosphere during the passage of a magnetic cloud. *Journal of Geophysical Research: Space Physics*, *126*(2), e2020JA028474.

Tanaka, Y.-M., Yumoto, K., Yoshikawa, A., Shinohara, M., Kawano, H., & Kitamura, T.-I. (2004). Longitudinal structure of pc3 pulsations on the ground near the magnetic equator. *Journal of Geophysical Research: Space Physics*, *109*(A3).

Turc, L., Zhou, H., Tarvus, V., Ala-Lahti, M., Battarbee, M., Pfau-Kempf, Y., ... others (2022). A global view of pc3 wave activity in near-earth space: results from hybrid-vlasov simulations. *Frontiers in Astronomy and Space Sciences*, 236.

Verhulst, T. G., & Stankov, S. M. (2020). Height dependency of solar eclipse effects: The ionospheric perspective. *Journal of Geophysical Research: Space Physics*, *125*(7), e2020JA028088.

Wang, H., & Lühr, H. (2007). Seasonal-longitudinal variation of substorm occurrence frequency: Evidence for ionospheric control. *Geophysical research letters*, *34*(7).

Wang, H., Lühr, H., Ma, S., & Ritter, P. (2005). Statistical study of the substorm onset: its dependence on solar wind parameters and solar illumination. In *Annales geophysicae* (Vol. 23, pp. 2069–2079).

Weimer, D. (1995). Models of high-latitude electric potentials derived with a least error fit of spherical harmonic coefficients. *Journal of Geophysical Research: Space Physics*, *100*(A10), 19595–19607.

Weimer, D. (2005a). Improved ionospheric electrodynamic models and application to calculating joule heating rates. *Journal of Geophysical Research: Space Physics*, *110*(A5). Retrieved from https://agupubs.onlinelibrary.wiley.com/doi/abs/10.1029/2004JA010884 doi: https://doi.org/10.1029/2004JA010884

Weimer, D. (2005b). Predicting surface geomagnetic variations using ionospheric electrodynamic models. *Journal of Geophysical Research: Space Physics*, *110*(A12). Retrieved from https://agupubs.onlinelibrary.wiley.com/doi/abs/10.1029/2005JA011270 doi: https://doi.org/10.1029/2005JA011270

Wu, C., Ridley, A., Goncharenko, L., & Chen, G. (2018). Gitm-data comparisons of the depletion and enhancement during the 2017 solar eclipse. *Geophysical Research Letters*, *45*(8), 3319–3327.

Yagova, N. V., Heilig, B., Pilipenko, V. A., Yoshikawa, A., Nosikova, N. S., Yumoto, K., & Reda, J. (2017). Nighttime pc3 pulsations: Mm100 and magdas observations. *Earth, Planets and Space*, *69*(1), 1–17.

Zhang, R., Le, H., Li, W., Ma, H., Yang, Y., Huang, H., ... others (2020). Multiple technique observations of the ionospheric responses to the 21 june 2020 solar eclipse. *Journal of geophysical research: space physics*, *125*(12), e2020JA028450.

Figure 1.

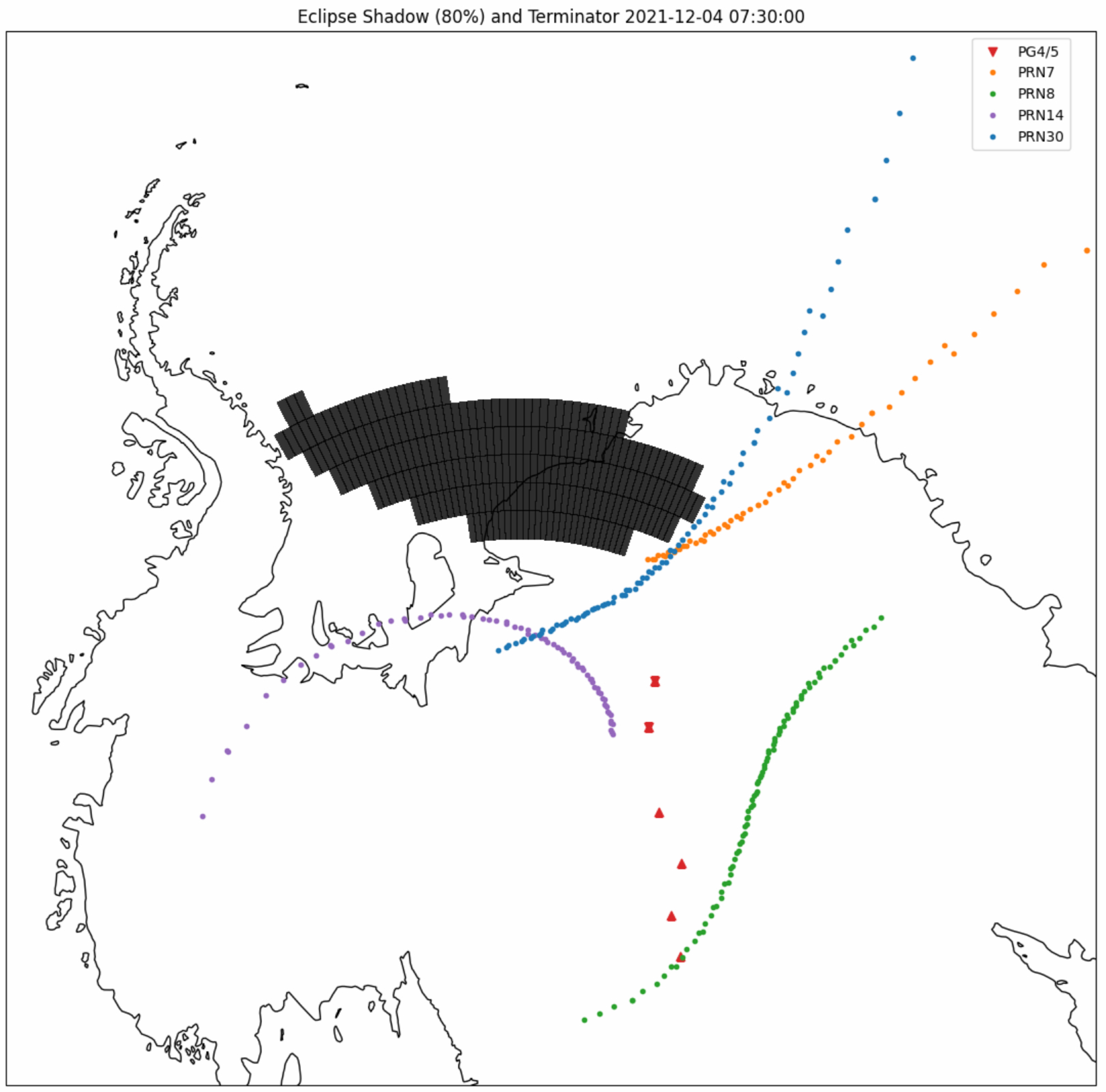

Eclipse Shadow (80%) and Terminator 2021-12-04 07:30:00
PG4/5
PRN7
PRN8
PRN14
PRN30

Figure 2.

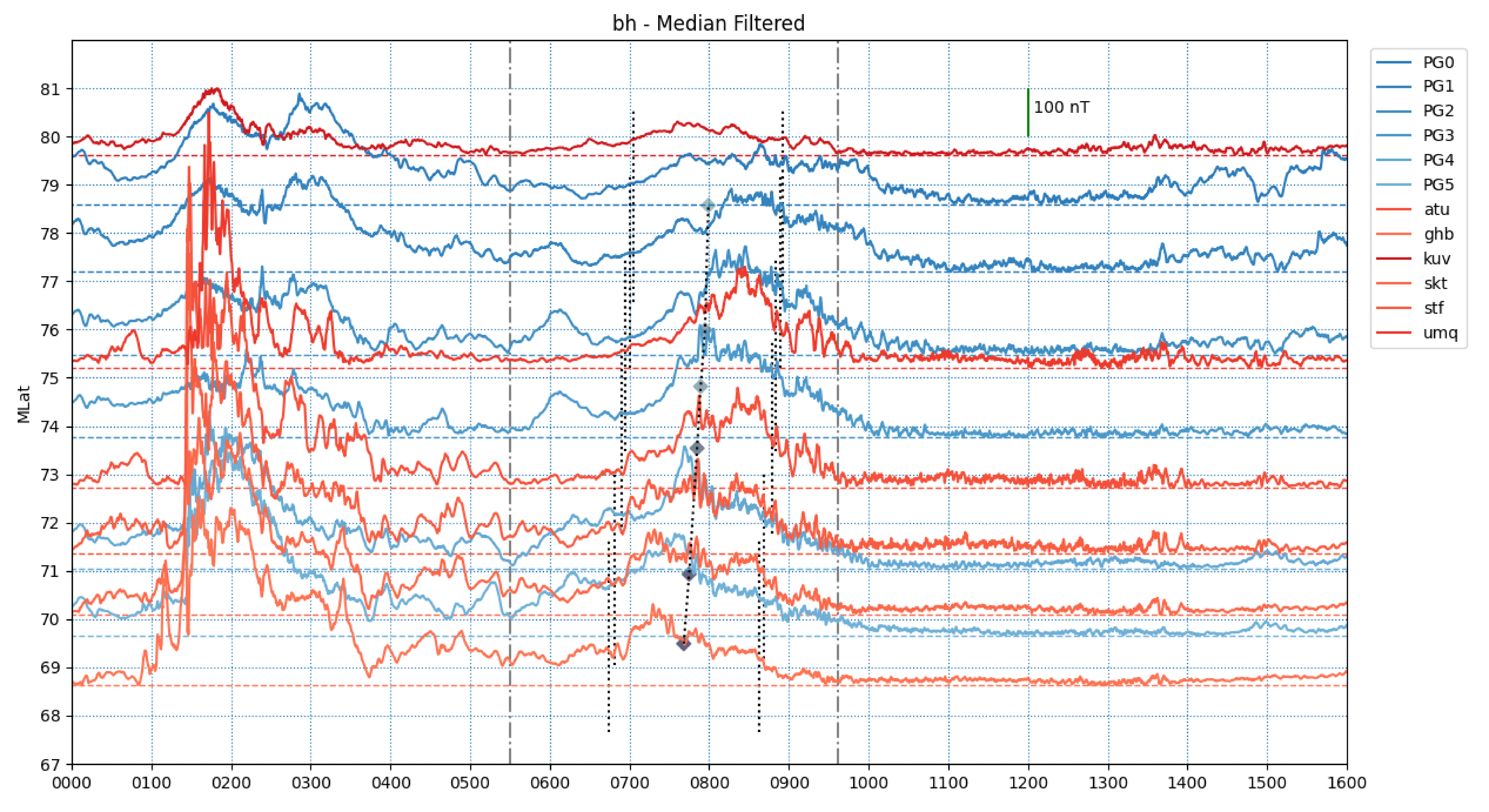
bh - Median Filtered
MLat
100 nT
PG0
PG1
PG2
PG3
PG4
PG5
atu
ghb
kuv
skt
stf
umq
81
80
79
78
77
76
75
74
73
72
71
70
69
68
67
0000
0100
0200
0300
0400
0500
0600
0700
0800
0900
1000
1100
1200
1300
1400
1500
1600

Figure 3.

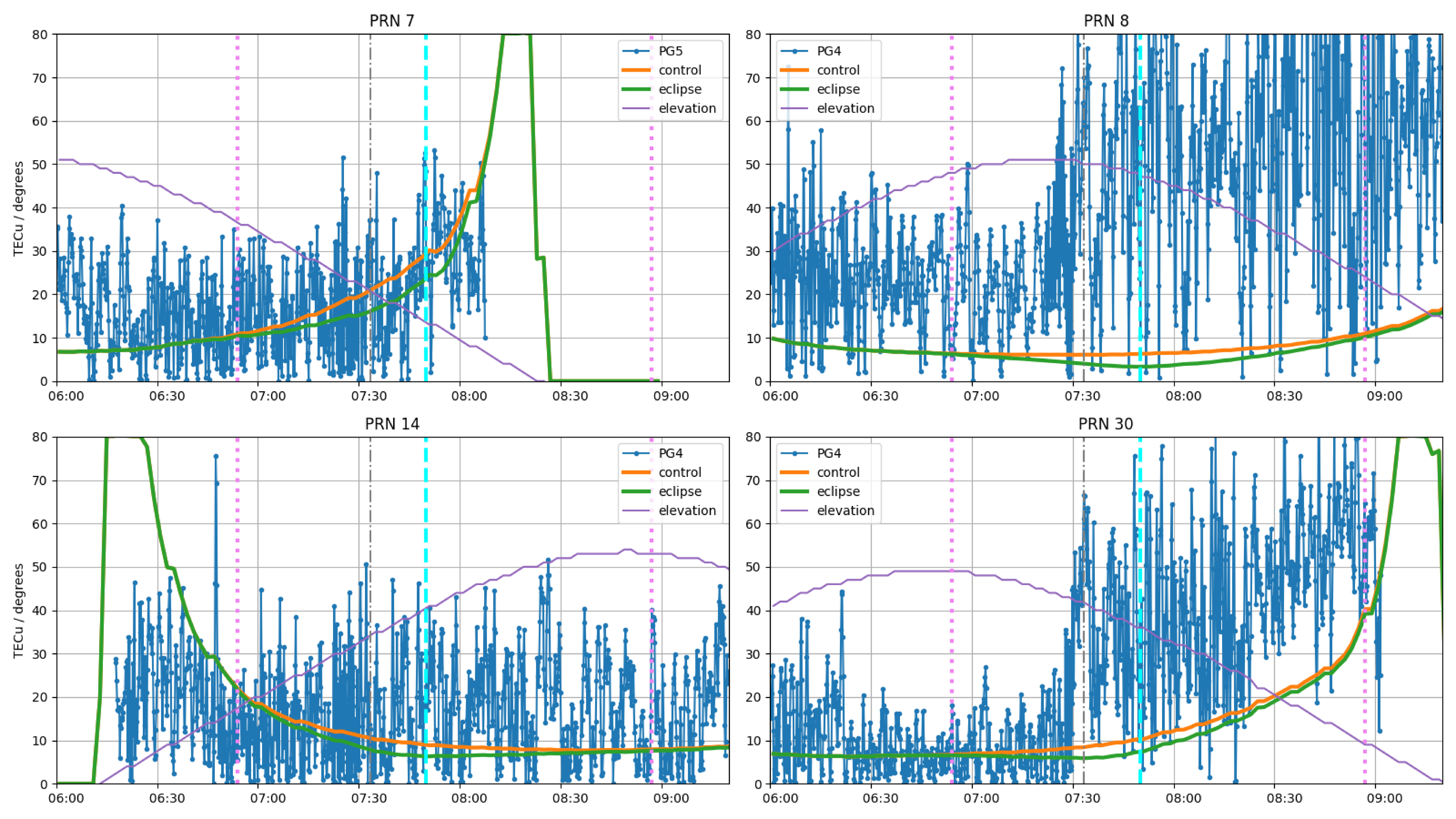
PRN 7
PRN 8
PRN 14
PRN 30
TECu / degrees
PG5
PG4
control
eclipse
elevation
06:00
06:30
07:00
07:30
08:00
08:30
09:00
0
10
20
30
40
50
60
70
80

Figure 4.

Satellite Vehicle: 7
Satellite Vehicle: 8
Satellite Vehicle: 14
Satellite Vehicle: 30
mHz
0
10
20
30
40
50
10^2
10^3
10^4
10^5
04 06:00
04 06:30
04 07:00
04 07:30
04 08:00
04 08:30
04 09:00

Figure 6.

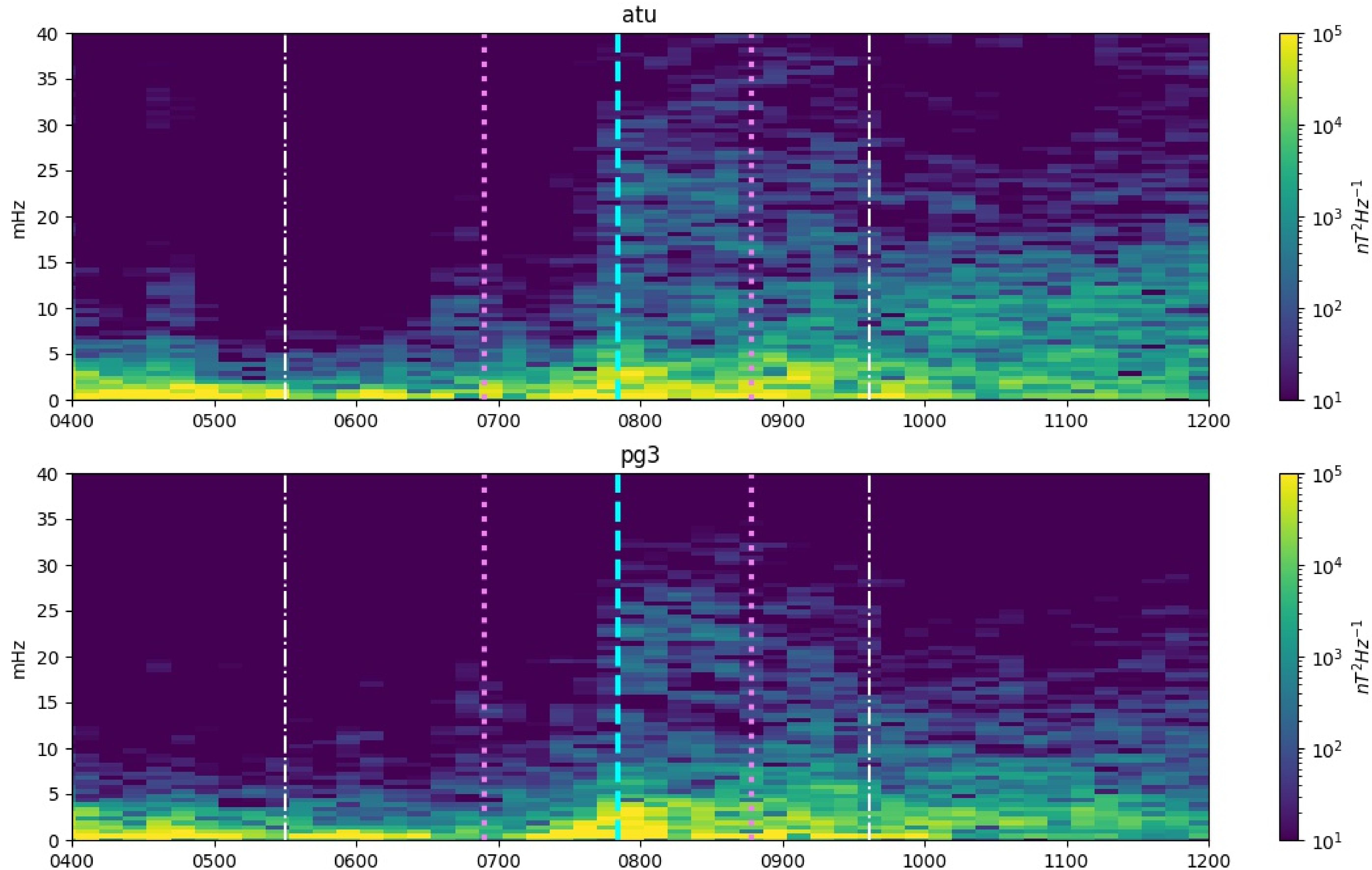

atu
pg3
mHz
40
35
30
25
20
15
10
5
0
0400
0500
0600
0700
0800
0900
1000
1100
1200
10^5
10^4
10^3
10^2
10^1
nT^2Hz^{-1}

Figure 6.

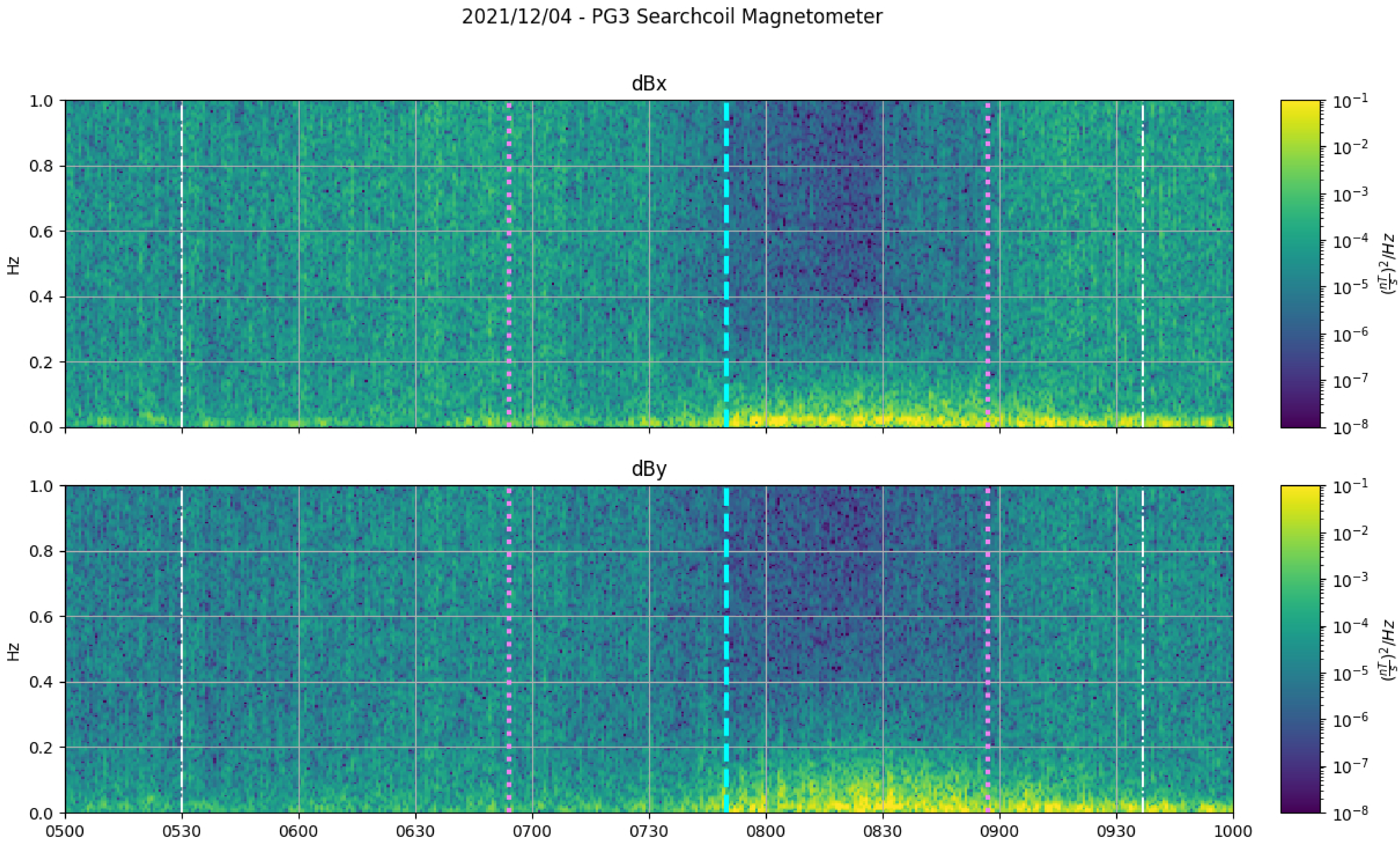

2021/12/04 - PG3 Searchcoil Magnetometer
dBx
dBy
Hz
1.0
0.8
0.6
0.4
0.2
0.0
0500
0530
0600
0630
0700
0730
0800
0830
0900
0930
1000
10^{-1}
10^{-2}
10^{-3}
10^{-4}
10^{-5}
10^{-6}
10^{-7}
10^{-8}
$(\frac{nT}{s})^2/Hz$

Figure 7.

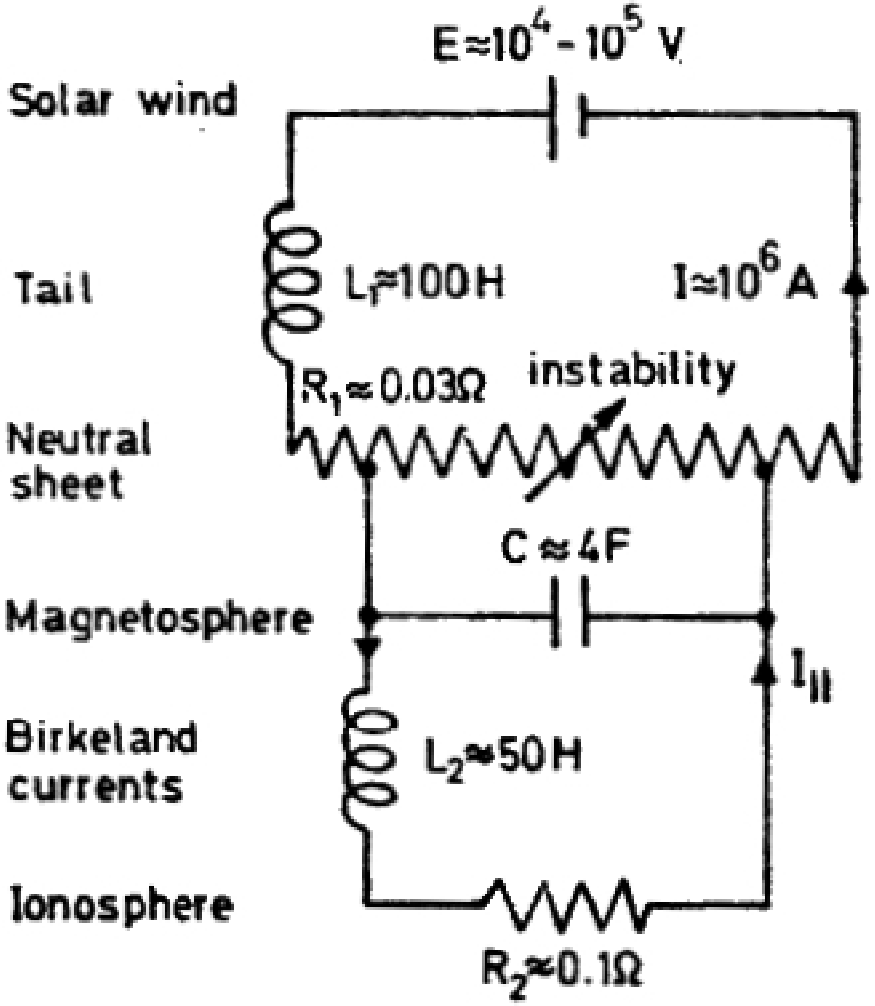

E≈10^4 - 10^5 V
Solar wind
Tail
L1≈100H
I≈10^6 A
R1≈0.03Ω
instability
Neutral sheet
C≈4F
Magnetosphere
I∥
Birkeland currents
L2≈50H
Ionosphere
R2≈0.1Ω

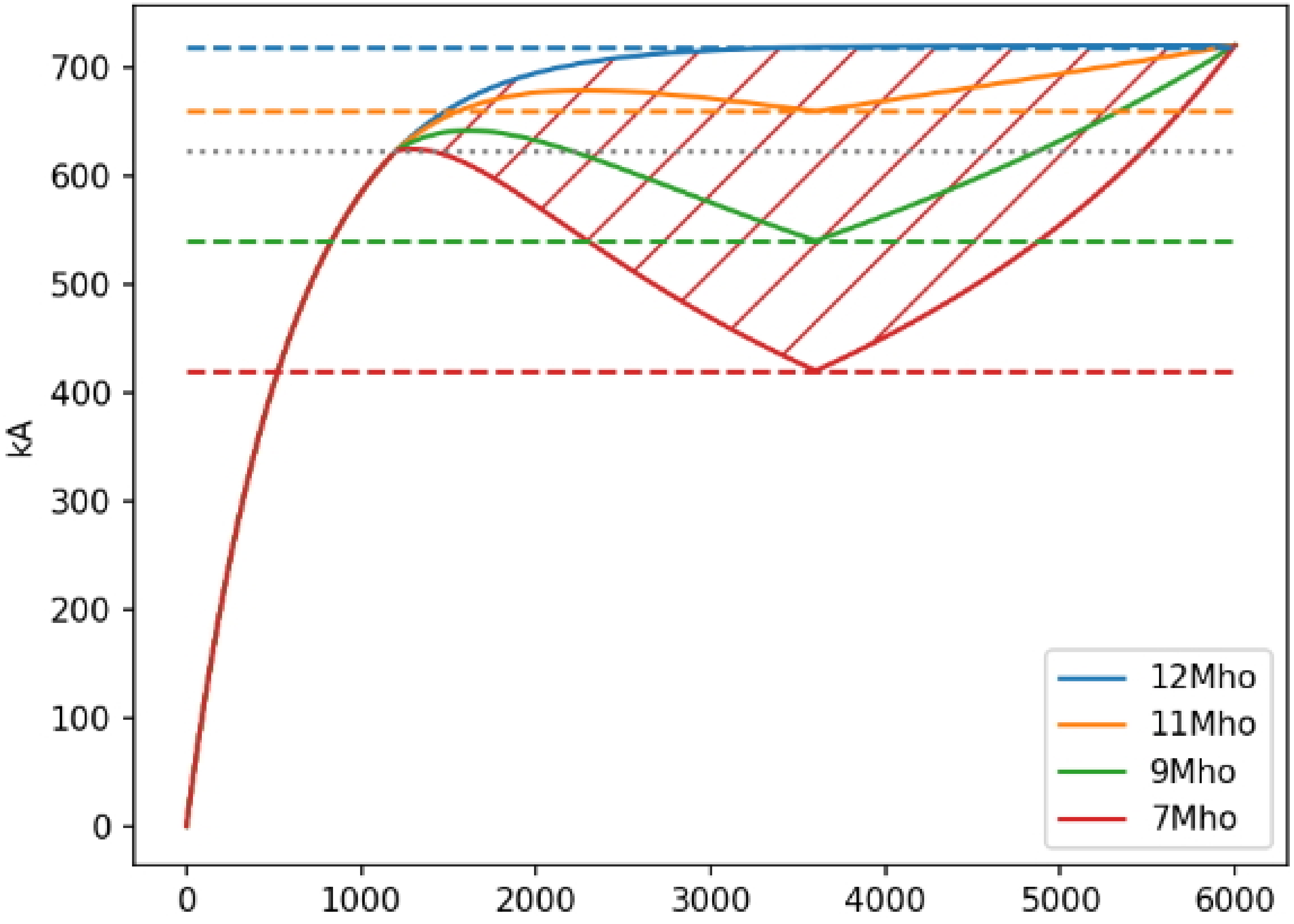

700
600
500
400
300
200
100
0
kA
0
1000
2000
3000
4000
5000
6000
12Mho
11Mho
9Mho
7Mho